Bifurcations in spiral tip dynamics induced by natural convection in the Belousov–Zhabotinsky reaction

Marcello Antonio Budroni,[1,a)] Marco Masia,[2] Mauro Rustici,[3,b)] Nadia Marchettini,[4] and Vitaly Volpert[5]
[1]*Dipartimento di Chimica, Università di Sassari, Via Vienna 2, I-07100 Sassari, Italy*
[2]*Dipartimento di Chimica, Università di Sassari, Via Vienna 2, I-07100 Sassari, Italy; CNR-INFM SLACS, Via Vienna 2, I-07100 Sassari, Italy; and INSTM, Via Vienna 2, I-07100 Sassari, Italy*
[3]*Dipartimento di Chimica, Università di Sassari, Via Vienna 2, I-07100 Sassari, Italy and INSTM, Via Vienna 2, 07100 Sassari, Italy*
[4]*Dip. Scienze e Tecnologie Chimiche e dei Biosistemi, Università di Siena, Via della Diana 2a, 53100 Siena, Italy*
[5]*Institut Camille Jordan, Université Claude Bernard Lyon 1, 43 boulevard du 11 novembre 1918, 69622 Villeurbanne cedex, France*

(Received 25 August 2008; accepted 26 November 2008; published online 12 January 2009)

The transition to spatial-temporal complexity exhibited by spiral waves under the effect of gravitational field in the Belousov–Zhabotinsky reaction is numerically studied on the basis of spiral tip dynamics. Successive transformations in tip trajectories are characterized as a function of the hydrodynamical parameter and attributed to a Ruelle–Takens–Newhouse scenario to chaos. The analysis describes the emergence of complexity in terms of the interplay between the evolution of the velocity field and concentration waves. In particular, (i) by mapping the tip motion in relation to some hydrodynamical pseudopotentials, the general mechanism by which the velocity field affects the tip trajectory is pointed out, and, (ii) by comparing the dynamical evolutions of local and mean properties associated with the inhomogeneous structures and to the velocity field, a surprising correlation is found. The results suggest that the reaction-diffusion-convection (RDC) coupling addresses the system to some general regimes, whose nature is imposed by the hydrodynamical contribution. More generally, RDC coupling would be formalized as the phenomenon that governs the system and drives it to chaos. © *2009 American Institute of Physics*. [DOI: 10.1063/1.3050356]

I. INTRODUCTION

In the past decades, pattern formation in active media has been a target of thorough studies. In particular, dynamics associated with spiral-like structures, resulting from characteristic properties of traveling waves, are remarkable examples of self-organization in excitable media.[1–4] Among them, one of the most well known is the Belousov–Zhabotisky (BZ) reaction.[5] It represents the typical nonlinear oscillating reaction in homogeneous phase, characterized by the alternation of two main processes by which a catalyst [typically cerium(IV) salts or ferroin] varies its oxidation state among $n+$ and $(n-1)+$.

The study of spiral waves in chemical systems has been traditionally carried out on gel matrices in order to bring the dynamics back to the simplified reaction-diffusion problem (RD systems).[6] Within this description, the system is modeled by a set of partial differential equations (PDEs), in which the kinetic functions, describing the chemistry, are coupled with the diffusive terms of the main species involved in the oscillating development of the reaction. A more general approach to the problem cannot neglect the influence exerted by the gravitational field on RD instabilities. Specifically, the onset of convective motions induced by the presence of density gradients and self-sustained flows arising from a reaction-diffusion-convection (RDC) coupling have to be considered. To this end, hydrodynamic equations are coupled to the RD PDEs: a set of nondimensional equations is derived taking into account gradients of density only ascribed to concentration inhomogeneities and controlled by a nondimensional parameter, the Grashof number, which determines the contribution of a particular species to convective motions.

By means of numerical studies, it has been extensively verified how the coupling between kinetic and transport phenomena in the BZ reaction can determine the formation of characteristic patterns[7–9] and how the development of instabilities associated with the hydrodynamics of the system would result in a transition to chemical chaos.[10–12] In particular, experimental observations coupled with theoretical results[13–17] demonstrate that natural convection can deform or even break spiral waves resulting into spatiotemporal chaos.

The time evolutions of a spiral wave could be followed in terms of the pattern its tip traces out. Transitions from simple rigid rotations around a small circular core to a quasiperiodic motion (typically along epicycle and meandering patterns) occur in tip trajectories as some parameters connected to the excitability of the system are varied.[18] In this paper, we present the influence of the convection on the spi-

[a)]Present address: Dip. Scienze e Tecnologie Chimiche e dei Biosistemi, Università di Siena, Via della Diana 2a, 53100 Siena, Italy.
[b)]Electronic mail: rustici@uniss.it.

ral wave properties in the BZ reaction through the analysis of the tip dynamics as a function of one hydrodynamical parameter: the Grashof number. The development to spatiotemporal chaos for rotating spiral waves is underlined by complex dynamics occurring in tip trajectories, culminating into a motion reminiscent of a random walk as the Grashof number is increased. Fast Fourier transforms (FFTs) and a topological analysis of minima and maxima of the stream function $\psi(x,y,t)$ (Sec. II A) are used to characterize, respectively, the Hopf bifurcations marking the passages from periodic to chaotic evolutions and the velocity field influence on spiral structures. There emerges a general mechanism by which the tip trajectory is related to transportation, distortions, and disruptions on spiral wave, induced by the velocity field. Evolutions of tip properties are also useful in highlighting the mutual correlation between the inhomogeneous structures and the velocity field arising for a suitable range of Grashof number values. The feature is specifically studied by comparing the following time series: (i) local dynamical properties [field velocity at each point visited by the tip during its evolution, $\mathbf{v}_{\mathrm{tip}}(t)$, versus tip velocity v_{tip}]; (ii) evolution in time of properties averaged in space ($\langle\langle\psi(x,y,t)\rangle\rangle$ versus $\langle c_i(x,y,t)\rangle\rangle$).

II. MODEL

In this section, we present the model used to describe the system dynamics and the method of analysis through which we could point out the features of the transition to spatial-temporal chaos.

A. RDC equations

Consider a two dimensional $(\hat{x},\hat{y})$ vertical slab, in which the gravitational field is directed along the $\hat{y}$ vertical axis. A set of PDEs to be solved by means of numerical integration over a square grid (100×100 points) is derived as in Ref. 10 by coupling the RD system to convection by the Navier–Stokes equations governing the velocity field in the slab. The set of PDEs formulated in the Boussinesq approximation[19] and written in the vorticity-stream function (ω-ψ) form is conveniently nondimensionalized by using the time scale $t_o=21$ s (Oregonator time unit) and a space scale $x_0=0.06$ cm.[10] Since it has been demonstrated that thermal gradients are negligible with respect to the concentration gradient for the onset of convection,[9,20,21] the hydrodynamic equations are formulated in the isothermal hypothesis. The resulting model is

$$\frac{\partial c_i}{\partial t}+D_\nu\left(u\frac{\partial c_i}{\partial x}+v\frac{\partial c_i}{\partial y}\right)-D_i\nabla^2 c_i=k_i(c_1,c_2),\quad i=1,2, \tag{1}$$

$$\frac{\partial \omega}{\partial t}+D_\nu\left(u\frac{\partial \omega}{\partial x}+v\frac{\partial \omega}{\partial y}\right)-D_\nu\nabla^2\omega=-D_\nu\sum_i \mathrm{Gr}_i\frac{\partial c_i}{\partial x}, \tag{2}$$

$$\frac{\partial^2\psi}{\partial x^2}+\frac{\partial^2\psi}{\partial y^2}=-\omega, \tag{3}$$

$$u=\frac{\partial\psi}{\partial y}, \tag{4}$$

$$v=-\frac{\partial\psi}{\partial x}, \tag{5}$$

where $k_i(c_1,c_2)$ are the kinetic functions which describe the oscillating behavior of the chemical species c_1 and c_2 within the Oregonator model:[22]

$$k_1(c_1,c_2)=\frac{dc_1}{dt}=\frac{1}{\epsilon}\left[c_1(1-c_1)+fc_2\frac{q-c_1}{q+c_2}\right], \tag{6}$$

$$k_2(c_1,c_2)=\frac{dc_2}{dt}=c_1-c_2. \tag{7}$$

The parameter values and the initial conditions are the same as in Ref. 10. For the sake of clarity in the discussion, we would like to stress the importance of the Grashof numbers and of the stream function.

- $\mathrm{Gr}_i=gx_0^3\delta\rho_i/\rho_i\nu^2$ is the Grashof number for the ith species (g is the gravitational acceleration (980 cm/s^2) and $\delta\rho_i/\rho_i$ is the density variation due to the change of the concentration of the ith species with respect to a reference value c_{0i}). This number is the control parameter chosen to follow the transition to chaos. It represents the intensity of convection only ascribed to isothermal density changes and is related to the hydrodynamic instability, giving the balance between momentum and viscosity forces acting in the system. In our simulations, the Grashof numbers for the two species are equal to each other.
- Formally, the stream function $\psi(x,y,t)$ is defined as the imaginary part of a complex potential, but, as shown in Eqs. (4) and (5), it could usefully be treated as a sort of velocity potential: by the $\psi(x,y,t)$ values at two different points, the associated velocity vector can be oriented and the flux through a line connecting the two points derived. Moreover, from Eq. (3) the relation existing between the curvature of the stream function along each direction and the vorticity ω can be noticed: in this way minima and maxima of $\psi(x,y,t)$ are related to regions of maximum intensity of fluid rotation and with vortex nature (given by the orientation of the vorticity z component) in those points.

The system of Eqs. (1)–(5) is solved numerically using the alternating direction finite difference method imposing no-slip boundary conditions for the fluid velocity and no-flux boundary conditions for chemical concentrations at the walls of the slab.

B. Analysis methods

In the first approach, the analysis points out the influence of the onset of convection on the spiral geometry and on the patterns described by the dynamics of the spiral tip. The tip position is analytically defined as the point of the spatial

domain where the cross product between the gradient vectors of the two species describing the kinetics, c_1 and c_2, is maximal:[23]

$$(\nabla c_1 \times \nabla c_2)_{x_{\text{tip}},y_{\text{tip}}} = \sup\{(\nabla c_1 \times \nabla c_2)_{i,j} \quad \forall\, i,j\}, \tag{8}$$

where i,j are the integer coordinates of the solving grid.

The tip dynamics is described by its coordinates, $\mathbf{x}_{\text{tip}}(t) = [x_{\text{tip}}(t), y_{\text{tip}}(t)]$, the velocity, $\mathbf{v}_{\text{tip}}(t) = [u_{\text{tip}}(t), v_{\text{tip}}(t)]$, and the distance from the origin, $d_{\text{tip}}(t) = |\mathbf{x}_{\text{tip}}(t)|$. When a significant coupling of the RD system with convection occurs, the definition given in Eq. (8) loses its unambiguous meaning due to distortions and possible breaks of the spiral wave. To identify the tip position, we scan the set of points derived from Eq. (8) considering the following additional assumptions:

(1) The tip belongs to the main arm of the spiral. By main arm, we mean the greater part of the wave in the system which conducts the general time evolution of the structure. The lifetime of the "islands" of concentration produced by the spiral breakdown is short, hinting that their role in the spiral evolution can be ignored.
(2) Continuity to the position of the spiral tip in the previous time step. Apart from the time intervals during which spiral breaks, the tip traces a continuous line and, at each time step, it has a high probability to be found close to its previous position.
(3) Contiguity to the $\psi(x,y,t)$ minimum closer to the spiral. As we will show below (Sec. III A), the $\psi(x,y,t)$ minima exert an attracting effect on the tip, driving its evolution. In this way, $\psi(x,y,t)$ minima are useful in detecting the tip position in the presence of spiral distortions and breaks.

These assumptions allow a reproducibility in almost 99% of cases, even for complex situations in which it is also very hard to refer to the structures as spirals.

The largest Lyapunov exponent has been calculated using the Kantz algorithm from TISEAN package.[24,25] The algorithm looks for exponential perturbation growth by implementing the formula

$$S(\epsilon,m,t) = \left\langle \ln\left(\frac{1}{U_n} \sum_{s_{n'} \in U_n} |s_{n+t} - s_{n'+t}| \right) \right\rangle_n, \tag{9}$$

where $s_{n'}$ represents a return point in the phase space close to the point s_n visited previously by the system; m is the embedding dimension and U_n the neighborhood with diameter ϵ. The maximal Lyapunov exponent λ is given by the slope of the pencil derived by $S(\epsilon,m,t)$ for different m, where it exhibits a linear increase, identical for each m.

III. RESULTS AND DISCUSSION

A. Topological analysis

The exploration of the tip dynamics as a function of the hydrodynamical parameter, the Grashof number, is carried out on the basis of the methods described in Sec. II B and of a topological analysis by which tip position is mapped in relation to $\psi(x,y,t)$ minima and maxima.

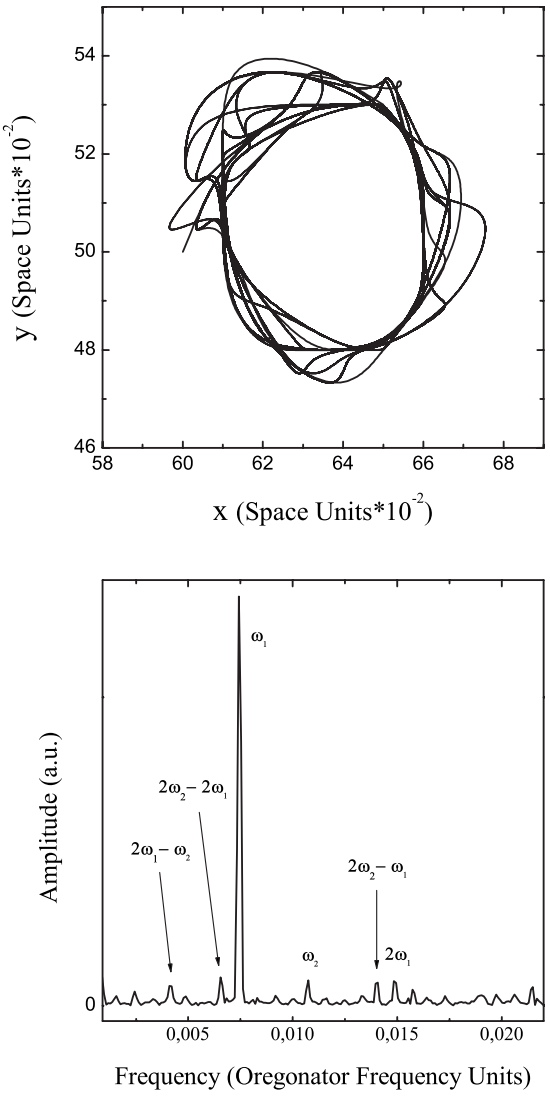

FIG. 1. Trajectory of spiral tip and FFT of its temporal evolution for quasiperiodic regime related to the simple RD problem ($\text{Gr}_i = 0.0$). The two incommensurable frequencies are $\omega_1 = 0.747$ O.F.U. and $\omega_2 = 1.071$ O.F.U.

1. $\text{Gr}_i = 0.0$

The system corresponds to a simple RD model. In this regime the hydrodynamic influence on spiral structures is absent: any distortions or breakdowns can be detected. The spiral tip localization reflects the traditional definition in Eq. (8). Following the trace of the points, it is observed that the initial setting of parameters places the system in a quasiperiodic starting condition as revealed by the main incommensurable frequencies, $\omega_1 = 0.747$ O.F.U. (Oregonator frequencies units) and $\omega_2 = 1.071$ O.F.U., found by the FFT analysis of the time series (Fig. 1). The nature of the dynamics observed is not surprising, since it is very close to what was found in Ref. 23 by varying the f parameter in a simple RD system. This regime is protracted for a range of values of the Grashof number up to 5.5, during which the tip dynamics and spiral structures do not appreciably suffer from the weak hydrodynamical field. In this first quasiperiodic domain, the characteristic frequencies differ in a negligible way from what is found for $\text{Gr}_i = 0.0$, with a decreasing trend in the absolute value of the main frequency and the entire dynamics close to a simple RD picture.

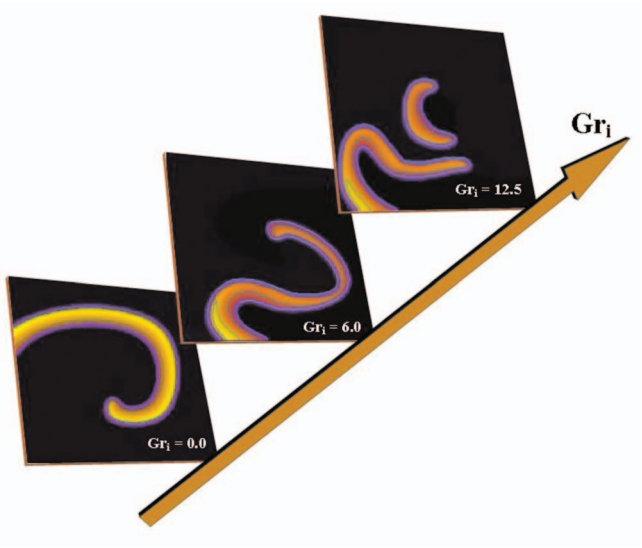

FIG. 2. (Color) Structural effect of velocity field in the spiral shape: $Gr_i=0.0$, the structure is unaffected by convective forcing; $Gr_i=6.0$, the wave is distorted; $Gr_i=9.8$, the velocity field is able to cause the break of the spiral structure.

2. $Gr_i=5.5$

The spirals are distorted by the velocity field but not yet subject to any breaking phenomena. Within these hydrodynamic conditions, the rising of the disturbing action of the field, whose destructive power will be shown for higher values of the Grashof number (Fig. 2), can be recognized. The dynamics shown by the tip motion in this regime is periodic. The tip follows a trajectory which approximates a closed cycle with a main frequency equal to 0.396 O.F.U. The transformation in the pattern type is concomitant with the emergence of an effective coupling between chemical and transport phenomena that produces characteristic RDC structures. The reduction in the absolute value of the main frequency (0.747–0.396) is associated with the hydrodynamical resistance, which cannot be neglected anymore (Fig. 3).

3. $Gr_i=9.8$

For values of Gr_i ranging between 9.8 and 12.1, the behavior exhibited by the spiral tip presents a degree of complexity which grows as Gr_i increases. It can be shown that the tip trajectory is connected to the following general mechanism (Fig. 4): the presence of a minimum in the $\psi(x,y,t)$ (in Fig. 4 plotted as contour level lines and indicated with solid arrows) acts as a sort of attracting potential, which "drives" the tip motion. This feature is related to the characteristics of the fluid in $\psi(x,y,t)$ minima. They represent the regions of high rotationality with negative vorticity able to accommodate spiral geometry and orient its evolution. The emergence of a maximum in the $\psi(x,y,t)$ function (dashed arrows in Fig. 4) causes the structure to break. It is interesting to point out how the spiral responds to the deforming and destructive action of the $\psi(x,y,t)$ maximum through an elastic dynamics: it flexes itself along the direction traced by $\psi(x,y,t)$ maximum; the resulting tip trajectory in the absence of $\psi(x,y,t)$ minima describes the same route as the maximum evolution. Also, these qualitative observations can be explained on the basis of the stream function features discussed in Sec. II A. In particular, $\psi(x,y,t)$ maxima represent vortex regions with positive vorticity and velocity field oriented in opposition to the spiral development, causing its disruption.

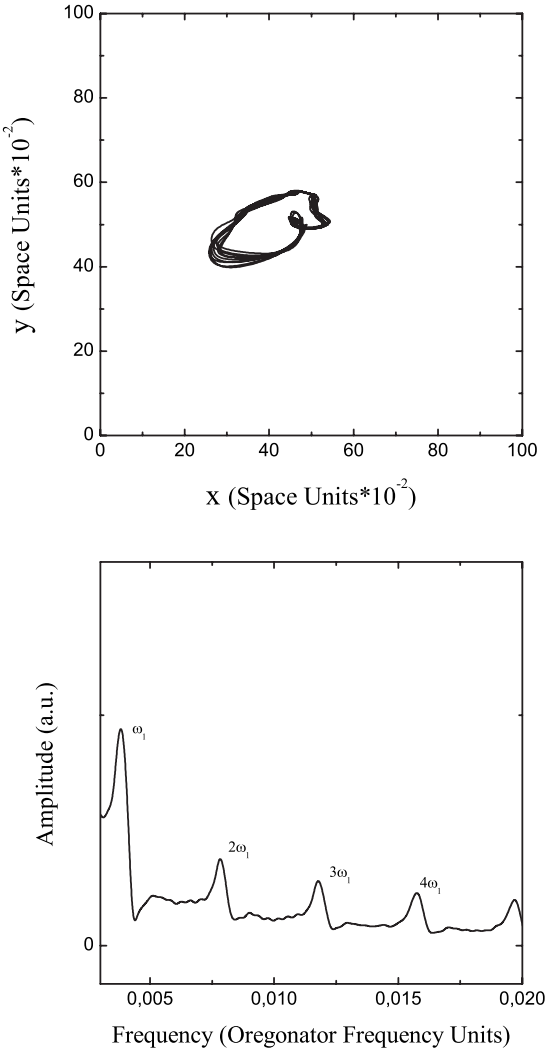

FIG. 3. Trajectory of spiral tip and FFT of its temporal evolution for the periodic regime ($Gr_i=6.0$). The main frequency is $\omega_1=0.396$ O.F.U.

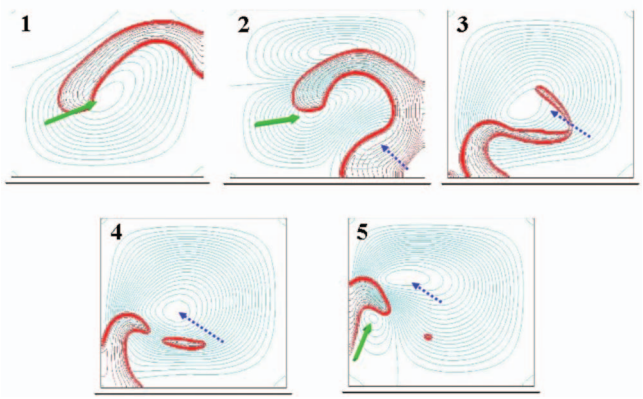

FIG. 4. (Color) Snapshots of the time evolution of $\psi(x,y,t)$ minima (solid line) and maxima (dashed line). The mechanism describes transport, distortion, and break of the spiral by fluid motion, determining the tip dynamics.

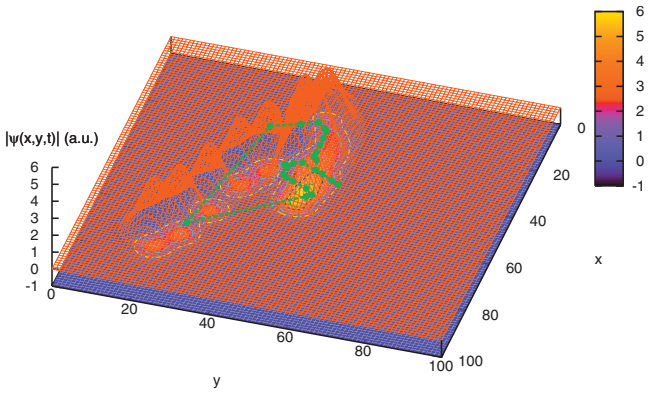

FIG. 5. (Color) Spatial-temporal evolutions of $\psi(x,y)$ minima and maxima, reported as absolute values (see Sec. III A). The trajectory described by the evolution of the two pseudopotentials reflects the tip pattern (line with points).

The mechanism involved in distortions, breaks, and transportation of the spiral structures, found for all of the hydrodynamical conditions considered, allows us to identify the type of action exerted by $\psi(x,y,t)$ minima and maxima on the wave.

Figure 5 presents graphically what the previous considerations implicate. We show the absolute values of $\psi(x,y,t)$ related to its minimum and/or maximum regions at some instants defining a complete cycle of the tip trajectory. The temporal evolution of these two pseudopotentials involves an alternation of two moments: the $\psi(x,y,t)$ maximum and the $\psi(x,y,t)$ minimum drifts. The figure, including the temporal dimension, reports a unique representation of the two drifts, hiding this dynamical feature. On the other hand, it stresses some spatial features, showing how the minimum drift [the one moving along the vector $\vec{s}_{\text{maximum}}=(15,43)\rightarrow(53,48)$] has a spatial development less prolonged than the maximum drift [which follows a displacement along $\vec{s}_{\text{minimum}}=(79,16)\rightarrow(37,38)$], even taking a shorter time (6×10^4 time steps versus 17×10^4). At each time step, a comparison between the tip position and the $\psi(x,y,t)$ maximum location outlines a delay due to the mechanism discussed above, while $\psi(x,y,t)$ minimum coordinates perform a complete overlap with the tip position during the complete evolution. The spatial distribution coming out as the sum of the two pseudopotential drifts traces a path in good agreement with the tip trajectory (dashed green line), as underlined by their projection. Figure 5 is useful in concluding that the pattern of tip dynamics could be effectively described as a combination of hydrodynamic processes that take place in the neighborhood of the spiral, namely, in terms of their spatial-temporal developments.

The Fourier transform of $d_{\text{tip}}(t)$ (Fig. 6) points out the presence of a Hopf bifurcation, detected by the emergence of a new frequency ($\omega_2=0.549$), whose ratio to the main one (seen for $\text{Gr}_i=5.5$) is an irrational number, and their harmonic combinations.

4. $\text{Gr}_i=12.1$

The tip trajectory can be referred to as a chaotic regime. The convective forcing determines a limiting hydrodynamical condition with respect to the persistence of spiral-like waves: the structures are broken in many residuals and are strongly distorted (Fig. 2). The tip dynamics is fitted to the evolution of the hydrodynamical pseudopotentials as discussed before (Fig. 7). An increased complexity, attributable to the presence of several residuals of spirals as well as to the coexistence of multiple minima and maxima of $\psi(x,y,t)$, hinders a detailed study.

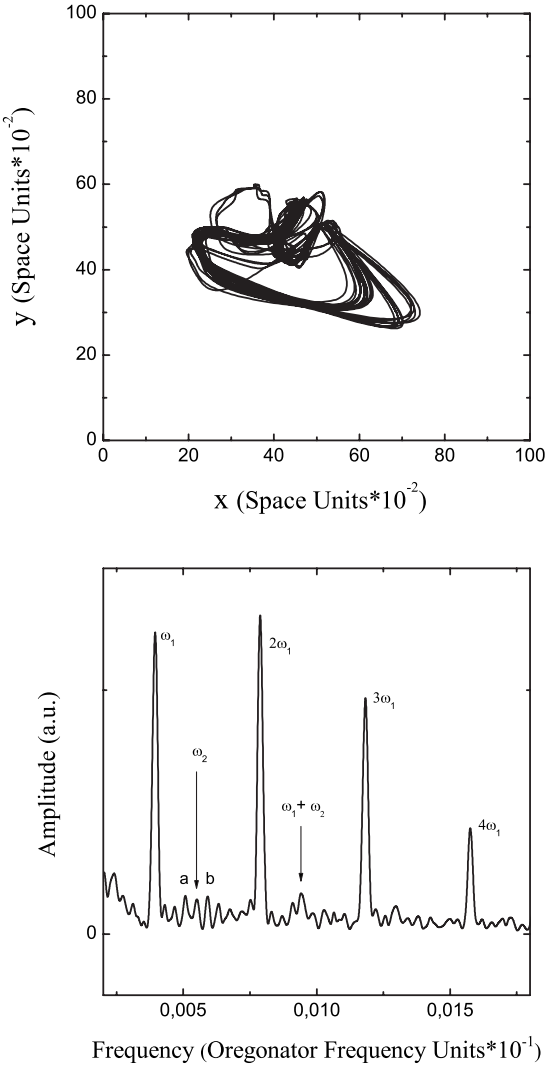

FIG. 6. Trajectory of spiral tip and FFT of its temporal evolution for the quasiperiodic regime ($\text{Gr}_i=9.8$). $a=6\omega_2-7\omega_1$, $b=\omega_1+1/2\omega_1$.

What follows from the analysis is a tip trajectory reminiscent of a random walk (Fig. 9), resulting in an aperiodic temporal series. Both the analysis of the maximum Lyapunov exponent, calculated as reported in Sec. III B [which presents a positive value equal to 0.2413 ± 0.0082 (Fig. 8)], and the Fourier transform [which evidences a spectrum with infinite frequencies and has major contribution at low values (Fig. 9)] clearly reveal the chaotic character of the dynamics.

From the discussed results, it could be stated that the analysis carried out represents a powerful tool to characterize the nature of the transition to spatial-temporal chaos, enabling us to attribute it to the Ruelle-Takens-Newhouse (RTN) scenario.

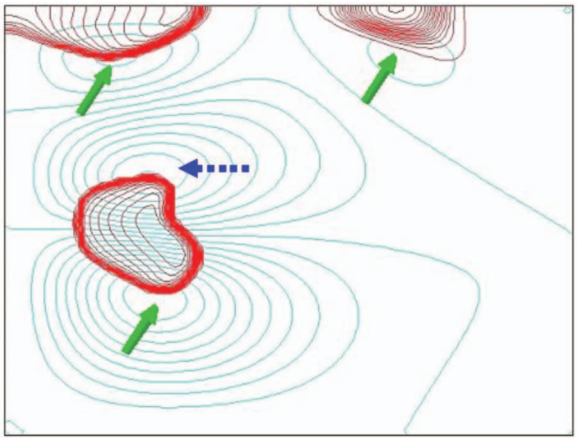

FIG. 7. (Color) Example of structural complexity associated with the emergence of multiple $\psi(x,y,t)$ minima (indicated by the dashed arrows), driving the spiral residuals.

B. The role of the RDC coupling

The previous topological analysis reveals how the tip study presents an intrinsic utility to describe the convective influence on spiral structures by the action of some pseudopotentials. We should consider the mutual influence determined by the dynamical feedback between the concentration inhomogeneities and the velocity field, generated by their interaction with the gravitational field.

The study of tip properties is useful also in characterizing this self-sustained mechanism and mutual correlation associated with it. We compare the time series reporting (i) the scalar values of the velocity field in the points visited by the tip during its time evolution at fixed Grashof number $[\mathbf{v}_{\mathrm{tip}}(t)]$ and (ii) the velocity of the tip, $v_{\mathrm{tip}}(t)$, calculated from the time series $d_{\mathrm{tip}}(t)$ (see Sec. II B) as

$$\frac{d_{\mathrm{tip}}(t_{i+1}) - d_{\mathrm{tip}}(t_i)}{\Delta t}, \tag{10}$$

where $\Delta t = 10^{-1}$ is the Oregonator time unit.

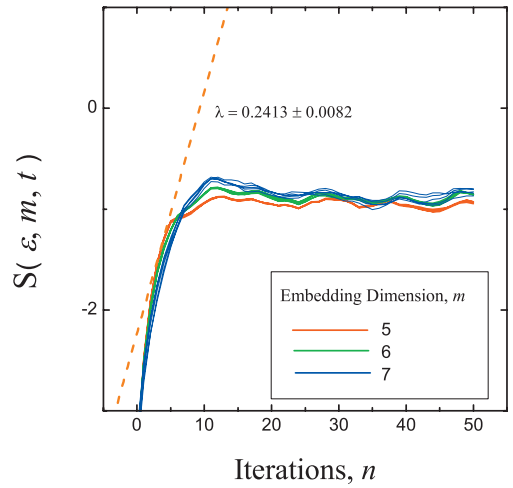

FIG. 8. (Color) Computation of the maximum exponent by the Kantz algorithm. The value of $\lambda = 0.2413 \pm 0.0082$ is obtained by the linear regression of the curves for $m = 5-7$ in the zone between two and five iterations.

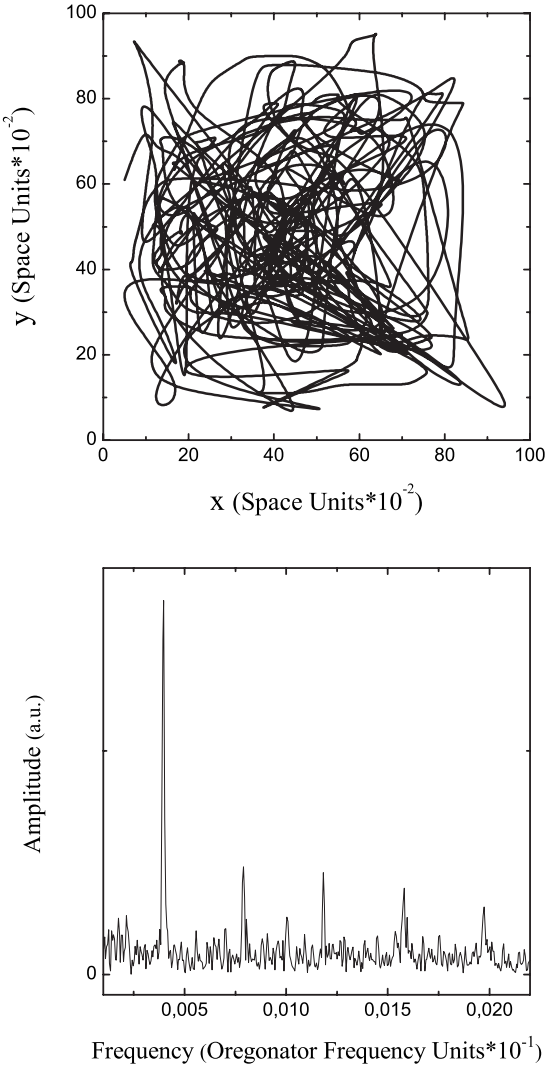

FIG. 9. Trajectory of spiral tip and FFT of its temporal evolution for chaotic regime ($\mathrm{Gr}_i = 12.1$).

In particular, the analysis is carried on FFTs of these series and reiterated for all of the stable regimes accessible to the tip dynamics as the controlling parameter (Gr_i) is increased.

In Fig. 10 an example of this sort of comparison concerns the quasiperiodic regime found for $\mathrm{Gr}_i = 9.8$. Two fundamental aspects are relevant: (i) there is complete overlapping of the two forms and (ii) the frequencies evidenced are the same as found in the FFT analysis of the time tip displacement (see Sec. III A). The repetitivity of this coherence for each hydrodynamic window explored and the recurrence in the specific values characterizing the regimes and the critical points allow us to extrapolate the strong correlation between the evolution of the velocity field, the tip behavior, and its velocity as a general property of the system.

The investigation could be extended to the time evolution of mean properties by considering the average of concentration $c_i(x,y,t)$ and the stream function $\psi(x,y,t)$ over the spatial domain (indicated as $\langle c_i(x,y,t)\rangle$ and $\langle \psi(x,y,t)\rangle$). Figure 11 describes the paths to chaos exhibited by the two observables when the Grashof number is varied; also in this

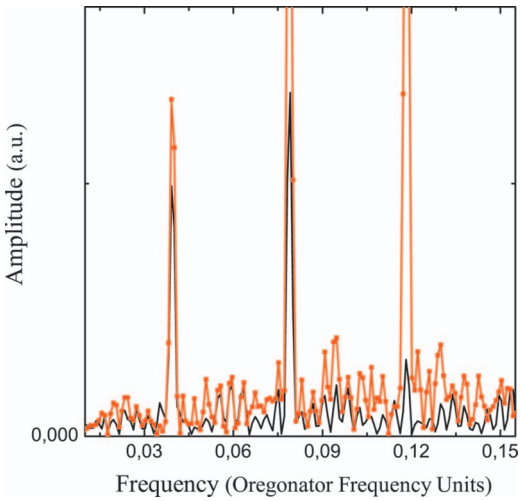

FIG. 10. (Color) Comparison between FFT of the time series of the velocity field considered in each point visited by the tip during its evolution and the tip velocity.

case a significant overlap in critical points of the bifurcation route and in characteristic frequencies defining each regime (see Table I) is found.

A detailed overview of the discussed behaviors is summarized in Table I. A part for a Grashof number ranging between 0.0 and 5.5 ($\langle c_i(x,y,t)\rangle$ is periodic while $d_{\mathrm{tip}}(t)$ is quasiperiodic, even with the same first main frequency), a strict congruence in the temporal evolutions involves all properties. The mismatch within this range underlines the indifference of tip dynamics and of $\langle c_i(x,y,t)\rangle$ to the velocity field. In other words a real RDC coupling cannot be recognized for a Grashof number ranging between 0.0 and 5.5: quasiperiodicity of tip trajectory and the periodicity of $\langle c_i(x,y,t)\rangle$ are to be referred to the simple RD system.

TABLE I. Dynamical regimes and main values characterizing the evolution of the dynamical and mean properties studied.

Gr_i	Properties	Regimes	Characteristic values
$0.0 \leq \mathrm{Gr}_i < 5.5$	$d_{\mathrm{tip}}(t)$	Quasiperiodic	$\omega_1=0.747,\ \omega_2=1.071$
	$\langle c_i(x,y,t)\rangle$	Periodic	$\omega_1=0.742$
	$\langle \psi(x,y,t)\rangle$	Periodic	$\omega_1=0.742$
$5.5 \leq \mathrm{Gr}_i < 9.8$	$d_{\mathrm{tip}}(t)$	Periodic	$\omega_1=0.396$
	$\langle c_i(x,y,t)\rangle$	Periodic	$\omega_1=0.396$
	$\langle \psi(x,y,t)\rangle$	Periodic	$\omega_1=0.396$
$9.8 \leq \mathrm{Gr}_i < 12.1$	$d_{\mathrm{tip}}(t)$	Quasiperiodic	$\omega_1=0.396,\ \omega_2=0.549$
	$\langle c_i(x,y,t)\rangle$	Quasiperiodic	$\omega_1=0.396,\ \omega_2=0.549$
	$\langle \psi(x,y,t)\rangle$	Quasiperiodic	$\omega_1=0.396,\ \omega_2=0.549$
$\mathrm{Gr}_i \geq 12.1$	$d_{\mathrm{tip}}(t)$	Chaotic	$\lambda=0.2413$
	$\langle c_i(x,y,t)\rangle$	Chaotic	$\lambda=0.0189$

It is surprising how the dynamical evolution of local properties and mean properties are close to the scenario to chemical chaos observed for the same system in our previous numerical work.[10] This coherence suggests the following considerations,

(1) The coupling of the chemistry of the system with the phenomena of mass transport can be considered as a dominant feature; it justifies the emergence of the same characteristic values for each dynamical profile under which the system is studied: chemical and/or hydrodynamical, either in spatial-averaged or in local properties. All of the dynamical features are ascribable to general regimes imposed to the system by the Grashof number.

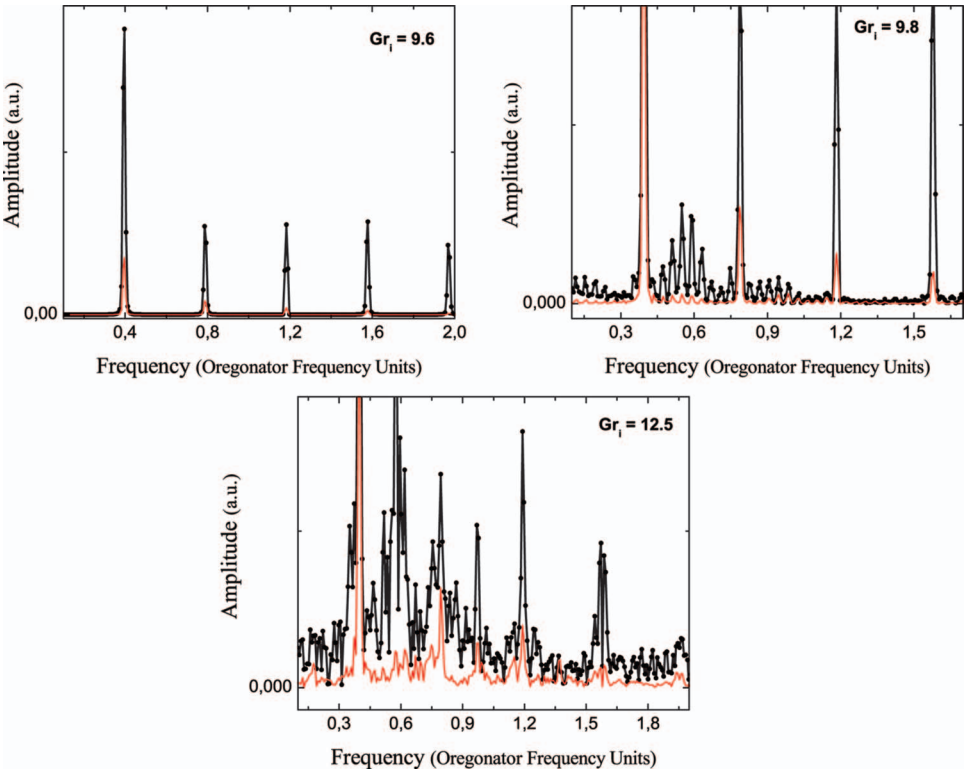

FIG. 11. (Color) FFT comparison between $\langle c_i(x,y,t)\rangle$ and $\langle \psi(x,y,t)\rangle$ in the evolution to chaos as Gr_i is increased. Critical points and emerging frequencies are superimposed.

(2) The coupling RDC determines the transition to chaotic dynamics for each characteristic. The general validity of this feature is given by the definite way by which each characteristic undergoes a chaotic regime, following a RTN scenario, as the Grashof number is increased. The nature of the route is mainly determined by the hydrodynamical contribution.

IV. CONCLUSIONS

The evolution of spiral waves within the BZ reaction under the effect of the gravitational field is studied numerically. To describe the transition to the spatiotemporal chaos observed numerically an analysis of the bifurcations occurring in spiral tip dynamics is carried out. In particular, tip trajectories as a function of the Grashof number are explored and characterized by FFT analysis of series reporting tip positions in time. The method allows a direct classification of the path to chaos as a RTN scenario, the bifurcation points being $\mathrm{Gr}_i=5.5$, $\mathrm{Gr}_i=9.8$, and $\mathrm{Gr}_i=12.5$ (respectively for the first subcritical Hopf bifurcation and the second and third supercritical Hopf bifurcations). The nature of the transition is analogous to the route to chemical chaos observed in Ref. 10 for the same system. The influence of the velocity field on spiral waves is outlined by studying the stream function properties. Specifically, by mapping the tip evolution in relation to the stream function dynamics, it has been shown how $\psi(x,y,t)$ minima can locate the tip in the presence of convective flows: they act as attractive potentials that, in the absence of $\psi(x,y,t)$ maxima, drive the tip motion. On the other side, $\psi(x,y,t)$ maxima present distortion and destructive power to which the spiral wave responds in an elastic way, until breaking. More importantly, this comparison highlights how the combined action of $\psi(x,y,t)$ minima and maxima fits the global tip trajectory. The general mechanism of transportation, distortions, and breaks by which the $\psi(x,y,t)$ minima and maxima exert their effect helps us understand bifurcations and regimes occurring in tip dynamics as $\psi(x,y,t)$ complexity increases. Besides describing convective influence on spiral structures, the tip analysis is also useful in studying the dynamical feedback existing between the inhomogeneous structures and the velocity field. As a matter of fact, the correlation between the two observables has been first pointed out by comparing the tip velocity and the velocity field in the positions visited by the tip in its evolution. The same investigation is extended to the dynamical behavior of mean properties ($\langle c_i(x,y,t)\rangle$ and $\langle\psi(x,y,t)\rangle$). Coinciding regimes and characteristic values emerge from two analyses. More generally, the given coherence permits us to conclude that (i) when a strong RDC coupling occurs, it dominates the evolution of the system, so that any dynamical property could be addressed to the stationary state imposed by the hydrodynamical control parameter and (ii) the RDC coupling is the potential source of transition to chaotic dynamics by a route determined by the hydrodynamical contribution.

ACKNOWLEDGMENTS

This research is supported by Università degli studi di Sassari (Grant No. FAR 2007), by Istituto Nazionale per la Scienza e Tecnologia dei Materiali (INSTM), and by Istituto Nazionale per la Fisica della Materia (CNR-INFM) at Sardinian Laboratory for Computational Materials Science, which are acknowledged. This work makes use also of results produced by the Cybersar Project managed by the Consorzio COSMOLAB, a project cofunded by the Italian Ministry of University and Research (MIUR) within the Programma Operativo Nazionale 2000–2006 "Ricerca Scientifica, Sviluppo Tecnologico, Alta Formazione" per le Regioni Italiane dell'Obiettivo 1 (Campania, Calabria, Puglia, Basilicata, Sicilia, Sardegna)—Asse II, Misura II.2 "Società 340 dell'Informazione," Azione a "Sistemi di calcolo e simulazione ad alte prestazioni." More information is available at http://www.cybersar.it. We gratefully acknowledge Luigi Ciotti for useful discussions.

[1] A. S. Mikhailov and K. Showalter, Phys. Rep. **425**, 79 (2006).
[2] A. Goldbeter, *Biochemical Oscillations and Cellular Rhythms* (Cambridge University Press, Cambridge, 1996).
[3] V. K. Vanag and I. R. Epstein, Proc. Natl. Acad. Sci. U.S.A. **100**, 14635 (2003).
[4] M. C. Cross and P. C. Hohenemberg, Rev. Mod. Phys. **65**, 851 (1993).
[5] A. N. Zaikin and A. M. Zhabotinsky, Nature (London) **225**, 535 (1970).
[6] S. K. Scott, *Oscillations, Waves and Chaos in Chemical Kinetics* (Oxford Chemistry Primers, Oxford, 1994).
[7] Yu. Gaponenko and V. Volpert, in *Patterns and Waves*, edited by A. Abramian, S. Vakulenko, and V. Volpert (St. Petersburg, 2003), pp. 292–309.
[8] Y. Wu, D. A. Vasquez, B. F. Edwards, and J. W. Wilder, Phys. Rev. E **51**, 1119 (1995).
[9] J. W. Wilder, B. F. Edwards, and D. A. Vasquez, Phys. Rev. A **45**, 2320 (1992).
[10] M. A. Budroni, M. Masia, M. Rustici, and N. Marchettini, V. Volpert, and P. C. Cresto, J. Chem. Phys. **128**, 111102 (2008).
[11] M. Rustici, M. Branca, C. Caravati, E. Petretto, and N. Marchettini, J. Phys. Chem. **103**, 6564 (1999).
[12] M. Masia, N. Marchettini, V. Zambrano, and M. Rustici, Chem. Phys. Lett. **341**, 285 (2001).
[13] J. I. Ramos, Chaos, Solitons Fractals **12**, 1897 (2001).
[14] J. N. Biktashev, A. V. Holden, and M. A. Tsyganov, Phys. Rev. Lett. **81**, 2815 (1998).
[15] V. Pérez-Villar, A. P. Mañzuri, M. N. Lorenzo, and V. Perez-Muñzuri, Phys, Rev. E **66**, 036309 (2002).
[16] K. I. Agladze, V. I. Krinsky, and A. M. Pertsov, Nature (London) **308**, 834 (1984).
[17] B. Sandstede, A. Scheel, and C. Wulff, J. Nonlinear Sci. **9**, 439 (1999).
[18] R. Kapral and K. Showalter, *Chemical Waves and Patterns* (Kluwer, Dordrecht, 1995).
[19] J. Boussinesq, Théorie Analytique de la Chaleur **2**, 172, Gauthier-Villars, Paris, 1903.
[20] K. A. Cliffe, S. J. Taverner, and H. Wilke, Phys. Fluids **10**, 730 (1998).
[21] M. Bockmann, B. Hess, and S. C. Muller, Phys. Rev. E **53**, 5498 (1996).
[22] *Oscillations and Travelling Waves in Chemical Systems*, edited by R. J. Field and M. Burger (Wiley, New York, 1985).
[23] W. Jahnke, W. E. Skaggs, and A. T. Winfree, J. Phys. Chem. **93**, 740 (1989).
[24] H. Kantz and T. Schreiber, *Nonlinear Time Series Analysis* (Cambridge Univesity Press, Cambridge, UK, 1997).
[25] The TISEAN software package is publicly available at http://www.mpipk-sdresden.mpg.de/~TISEAN.